Indian Journal of Engineering & Materials Sciences
Vol. 29, August 2022, pp. 540-549
DOI: 10.56042/ijems.v29i4.47785

Hardness and corrosion resistance of Zn−Mn/Al_2O_3 composite coatings produced by electrochemical deposition

Mihael Bučko[a*], Marija Riđošić[b], Jovanka Kovačina[c], Milorad V Tomić[b], & Jelena B Bajat[d]

[a]Universitys of Defense, Military Academy, Pavla Jurišića Šturma 33, 11000, Belgrade, Serbia

[b]University of Eastern Sarajevo, Faculty of Technology Zvornik, Karakaj 34A, 75400 Zvornik, Republic of Srpska, Bosnia and Herzegovina

[c]Institute of Chemistry, Technology and Metallurgy, Njegoševa 12, 11000 Belgrade, Serbia

[d]Faculty of Technology and Metallurgy, University of Belgrade, P O Box 3503, 11120 Belgrade Serbia

Received: 22 March 2021; Accepted: 31 August 2021

The aim of this study is development and characterization of the novel Zn-Mn/Al_2O_3 composite coatings. The coatings were electrodeposited with constant current density on steel, from chloride solution, without any commercial additives. The Zn−Mn alloy coatings that show high corrosion resistance, may be used in future as an alternative to cadmium coatings. However, the pure Zn and Zn alloy coatings are characterized with poor mechanical properties. Therefore, in this work the alumina particles were incorporated into the Zn-Mn matrix, and the hardness and corrosion resistance of the obtained composite coatings were tested. The mechanical and ultrasound agitation were used to achieve good dispersion of plating solution and homogeneous co-deposition of second phase. The goal was to examine the effect of the agitation type in bath, on the attributes of the deposited composite coatings. The incorporation of Al_2O_3 particles was enhanced when the mechanical agitation of the solution was applied. However, in case that this agitation method was used, the agglomeration of the alumina particles occurred. In contrast, when an ultrasonic agitation of the plating solution was applied, the uniform distribution of the alumina particles could be achieved. The presence of particles in the matrix, along with applied ultrasound, resulted in grain refinement and homogeneous microstructure. The Al_2O_3 nanoparticles incorporated in Zn-Mn alloy matrix, resulted in a significant increment in the indentation hardness and a modest increase in the coating corrosion resistance. However, the coating hardness increased with alumina addition, only in case when an ultrasonic agitation of the electrodeposition solution was used.

Keywords: Zn alloys, Alumina, Composite materials, Nanoindentation, Corrosion resistance

1 Introduction

Zinc coating has been widely applied in the corrosion protection of steel substrate since the 1960s. The application of the Zn coatings is found in the construction pieces, automobile industry, general mechanics and electronic components.

With the goal of improving the structure and the properties of the coating, such as morphology, microhardness, fracture strength, wear and corrosion resistance, a great research progress was made in the electrochemical deposition of Zn alloy and Zn composite coatings in the past decades[1]. The Zn alloy coatings that have found the broadest application range are Zn−Ni, Zn−Fe, Zn−Co, Zn−Sn and Zn−Mn alloy. On the other hand, the Zn composite coatings are obtained by using electroplating baths with various dispersive fine phases, for instance Si_3N_4, SiC, MoS_2, SiO_2, TiO_2, and Al_2O_3, and soft phases, for example graphene and polytetrafluoroethylene (PTFE). The size and content of the added particles, and their distribution in the metallic matrix, significantly influence various characteristics of the composite coating[2].

The improvement of different features of a composite coating depends mainly on the size and the percentage of the incorporated fine particles, as well as on their distribution in the metallic matrix[2].

The aim of this work has been the production of a new Zn−alloy−composite coating, i.e. the coating that will benefit from the insertion of both an additional metal and a ceramic particle into the zinc matrix. A number of Zn based coatings of this type have been produced by electrodeposition until now, for example Zn−Ni/Al_2O_3[3], Zn–Ni/carbon nanotubes (CNT)[4], Zn−Ni−P/CNT, Zn−Fe−P/CNT[5], Zn−Co/CNT[6], Zn−Co/TiO_2[7], etc.

In spite of the previous enormous work, to the best of our knowledge very little research has been published on

* Corresponding author (E-mail: mbucko@tmf.bg.ac.rs)

the electrodeposition of Zn−Mn−composite coatings until now. As a matter of fact, the literature search shows only the report on the fabrication of Zn−Mn/Stabilized Polymeric Micelles (SPM)[8] composite coating. This is surprising, because the Zn–Mn alloys were reported to possess better corrosion resistance as compared to other Zn alloys, especially in aggressive media that contain NaCl and SO_2 compounds[9]. Namely, it is well known that the insoluble basic Zn salts or Mn oxides that are formed on the coating surface, are responsible for a high corrosion resistance of Zn–Mn coatings in aggressive media[10].

Bearing in mind the high corrosion performance of Zn–Mn alloy, this work investigates the possibility of electrodeposition of composite Zn–Mn/Al_2O_3 coating. The Al_2O_3 possesses high resistance toward temperature, acids, and bases, and good mechanical properties, such as significant hardness and wear resistance. For these reasons, this compound has often been applied in various metallic composite materials[2]. A few examples of composite coatings that contain Al_2O_3, include Cu/Al_2O_3, Au/Al_2O_3, Ni/Al_2O_3[2], Ag/Al_2O_3[11], and Co−W/Al_2O_3[12].

Therefore, the present study is focused on two goals: (1) probing the electrodeposition of Zn−Mn/Al_2O_3 composite coatings from chloride bath and (2) characterizing the obtained coatings in terms of their morphology, hardness, and corrosion resistance.

2 Materials and Methods

2. 1. Electrodeposition of composite coatings

Adequate Zn−Mn/Al_2O_3 composite coatings were electrolytically deposited from a chloride bath to which Al_2O_3 powder with an average particle size of 0.3 μm (according to the commercial supplier, Buehler) was added in concentration of 1.0 g dm^{-3}. To avoid agglomeration after alumina was added, the suspension was intensively agitated by a magnetic stirrer (300 rpm) for at least 2 h at room temperature before the codeposition experiments. The chloride bath composition was as follows: KCl 1.8 mol dm^{-3}, $ZnCl_2$ 0.45 mol dm^{-3}, $MnCl_2$ 0.45 mol dm^{-3} and H_3BO_3 0.4 mol dm^{-3}. All chemicals were of analytical grade, supplied by Sigma-Aldrich. In order to focus on the changes that result from the Al_2O_3 present in the bath, the addition of plating additives was avoided.

The codeposition experiments were performed in a 200 ml volume cylindrical glass cell. Coatings were deposited on mild steel coupons of 8 cm^2. The anode was a pure Zn foil (20 cm^2), and saturated calomel electrode (SCE) was the reference electrode. The substrates were polished with 800, 1200 and 2000 emery grade paper, degreased in ethanol, rinsed in distilled water, pickled in a 20% HCl solution (10 seconds) and rinsed again. Electrodeposition was carried out at a constant current density of 40 or 50 mA cm^{-2} using PAR M173 galvanostat as a power supply, with 22 C cm^{-2} of total charge passed, in order to obtain 10 μm thick coatings. To maintain a uniform alumina particle concentration in the bulk solution and to enable a good convection towards the cathode, two agitation methods were used during the electrodeposition process: agitation by a magnetic stirrer (w=300 rpm), and ultrasonic energy by an ultrasonic bath (24 kHz).

The electrolyte temperature was maintained at 25 °C. Electrochemical cell was thermostated in order to prevent temperature increase due to ultrasonic energy. The obtained samples were immersed in ethanol for 1 min and dried.

2. 2. Coating characterization

An energy dispersive X-ray spectrometer (EDS), INCAPenta-FETex3, Oxford Instruments, was used for chemical analysis of the deposits. The chemical composition was examined at four different locations of each coating and the average weight percentage of Zn, Mn, O, and Al_2O_3 incorporation was calculated. An optical microscope Olympus CX 41, with microscope camera Olympus UC 30, and scanning electron microscope FEI Quanta 200, were used to characterize the morphology of the deposits.

The hardness of the Zn−Mn alloy and Zn−Mn/Al_2O_3 composite coatings was investigated by means of nanoindentation experiments, using Anton Paar nanoindentation tester. The nanoindenter contains a Berkovich three-sided diamond pyramid with centerline-to-face angle 65.3° and 20 nm radius at the indenter tip. Series of 6 indentations were made on each sample (6 loading-unloading cycles) with control of the load (maximum load 50 mN), the loading and unloading rate of 100.00 mN min^{-1} and 15 s peak hold time at maximum load.

For corrosion measurements, the samples were immersed in a neutral 0.3 wt. % NaCl solution at 25 ^oC for various time periods. The experiments were performed in a 250 ml volume Teflon cell, using Pt mesh and a SCE as auxiliary and reference electrodes, respectively. One of the Teflon cell's walls contains a

drilled hole of 1 cm^2, and the working electrode was pressed with the hole from the outer side of the cell, so that the electrolyte was in contact only with 1 cm^2 of the exposed electrode surface. Rubber ring sealant was used to prevent electrolyte leakage between the cell and the electrode.

The investigation of the behavior of the coatings in NaCl solution was performed by electrochemical impedance spectroscopy (EIS) and polarization measurements. AC impedance spectra were measured at the OCP after certain immersion times, using a potentiostat ZRA Reference 600, Gamry Instruments. The impedance spectra were recorded in the frequency range between 100.000 and 0.01 Hz, at 10 frequency points per decade, with 10 mV amplitude perturbing signal. Echem Analyst software was used for the fitting.

The potentiodynamic polarization curves were obtained after establishing stable open circuit potential (~60 min after immersion), with the scan rate of 0.25 mV s^{-1}, ±250 mV vs. OCP, from negative to positive potential limit. The electrochemical parameters of the corrosion process were extracted from the polarization curves by using DC Corrosion Software (Gamry Instruments). To ensure a proper reproducibility, the corrosion experiments were performed two or three times.

3 Results and Discussion

3. 1 Chemical composition and surface morphology of the coatings

In order to analyze the effect of various electrochemical deposition parameters on the Al_2O_3 and Mn content in the Zn−Mn alloy and Zn−Mn/Al_2O_3 composite coatings, the coatings were deposited at different current densities, with magnetic stirrer or ultrasonic agitation. The chemical composition obtained is presented in Table 1.

The manganese content in the deposits increases slightly with the deposition current density, the effect well known from earlier work on Zn−Mn electrodeposition[9,10]. The oxygen percentage in all samples varies between 9 and 13 wt.%, and this oxygen is the result of the surface oxidation of the coatings prior to their EDS analysis, plus the oxygen present in alumina particles.

Table 1 evidences that the content of the incorporated Al_2O_3 particles strongly depends on the agitation type of the electrolyte: the mechanical agitation with magnetic stirrer enables incorporation of more than twice as high amount of Al_2O_3 as compared to the ultrasonic agitation. It is also noted that a deposition current density affects the alumina content, since the increase in deposition current density resulted in a low increment of Al_2O_3 content in the coatings.

It is interesting to note that in previous works where the type of agitation was compared, the composite coatings obtained under ultrasonic agitation contained higher percentage of Al_2O_3 in comparison to those obtained by mechanical stirring[13]. The composite material is formed in a manner that the alumina particles are transported to the cathode surface by bath agitation, and then the particle occlusion by metallic atoms occurs, as a result of the electroreduction of the adsorbed metal ions[14]. The higher level of particle incorporation observed under ultrasonic agitation had been attributed to the more effective particle dispersion and deagglomeration through the application of ultrasound that leads to an increased number of particles that may be occluded in the metal coating[13].

In our experiments, however, the stronger convection of the electrolyte and promotion of the particle transport to the cathode surface was evidently achieved by magnetic stirrer, resulting in a higher content of Al_2O_3 in the coatings. However, a significantly more successful deagglomeration and dispersion were accomplished by ultrasound, resulting in a clearly more homogenous distribution of the alumina particles in the matrix, as indicated by the optical microscope images in Fig. 1.

At optical microscope images it was observed that the surface of all samples showed non-porous and

Table 1 — Chemical composition of Zn−Mn and Zn−Mn/Al_2O_3 coatings

Sample No.	Deposition c.d.	Deposition conditions	wt.% Mn	wt.% Al	Calculated wt.% Al_2O_3	wt.% O
1	50 mA cm^{-2}	magnetic stirrer	5.8	0	0	12.2
2	40 mA cm^{-2}		5.2	0	0	11.5
3	50 mA cm^{-2}	magnetic stirrer + Al_2O_3	5.3	2.6	4.8	13.8
4	40 mA cm^{-2}		4.7	2.4	4.5	11.0
5	50 mA cm^{-2}	ultrasound + Al_2O_3	5.9	1.0	1.8	12.8
6	40 mA cm^{-2}		4.9	0.7	1.3	9.7

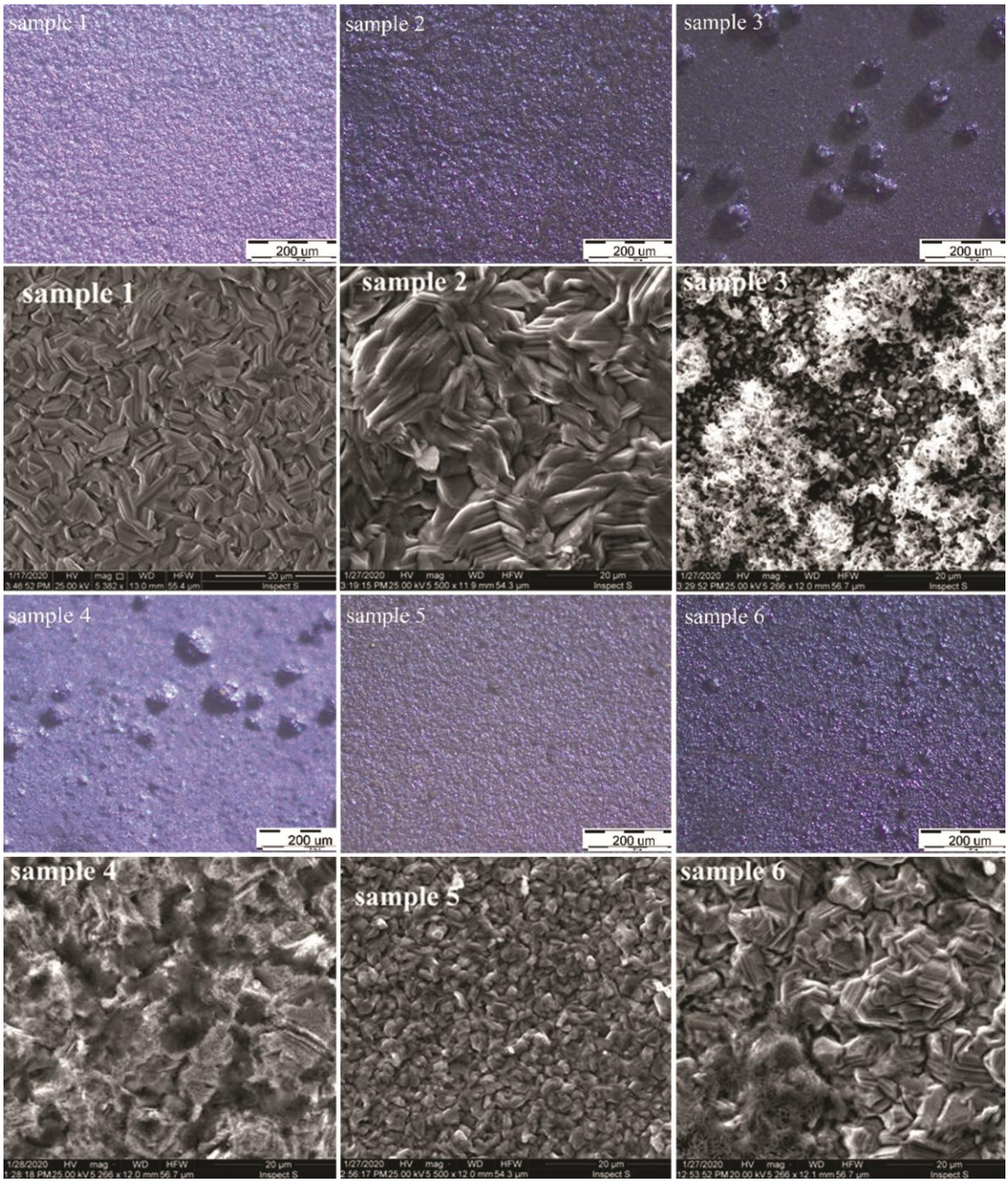

Fig. 1 — Optical images presenting the surface morphology of the Zn−Mn and Zn−Mn/Al_2O_3 coatings deposited under various parameters, the samples designation is the same as in Table 1.

compact structure formed by dissimilar agglomerates. When Al_2O_3 particles were added to the electrolyte, and mechanical agitation was applied, the coating contained two layers: the compact layer adhering to the steel substrate, and the upper layer made of the agglomerated codeposited particles, in the form of randomly distributed aggregates with up to 50 µm in diameter (samples 3 and 4). When ultrasonic agitation was applied (samples 5 and 6), the aggregate particles were discernible, but were smaller and more homogeneously dispersed in the metal matrix. Similar results have been reported earlier[13].

The influence of the incorporated particles on the coatings microstructure is better seen on SEM images in Fig. 1. The presence of the particles undoubtedly affected microstructure of the matrix. As can be seen,

the agglomerate size of all samples containing particles (Samples 3-6) decreased. The incorporation of the particles in deposit increases the number of nucleation sites resulting in the growth of grain agglomerates with more regular size and shapes[13]. Presented SEM images showed that topography was influenced by deposition current density, the higher the current density the smaller the agglomerate size (Samples 1, 3 and 5 compared to Samples 2, 4 and 6). The magnetic stirring resulted in heterogeneous morphology and rough surface finish (Samples 3 and 4). When ultrasound is applied in the plating solution, different cavitation phenomenon and micro-turbulence are present, like acoustic streaming, shock-waives, acoustic streaming, etc.[15,16]. As a consequence, the hydrogen bubbles formed on the cathode surface are easily removed and avoiding the bubbles incorporation into deposit enhances the compactness of the composite coatings. Such acoustic phenomenon easily breaks bonds between particles in agglomerates, thus enhancing homogeneous distribution of particles in solution[15].

In SEM microphotographs of the samples 3 and 4, the inhomogeneous morphology may be noticed. The EDS analysis of white deposits emerging on the surface confirmed that they were aggregated alumina particles that were not well incorporated into the alloy matrix. The EDS analysis of other samples did not indicate the presence of such heterogeneous inclusions, so we conclude that the alumina particles were evenly dispersed in those samples.

3. 2 Hardness of the coatings

The indentation hardness (H_{IT}) and Vickers instrumented hardness (HV_{IT}) of the Zn−Mn and Zn−Mn/Al_2O_3 coatings were calculated from nanoindentation measurements, following the Oliver & Pharr approximation method. The obtained results are presented in Fig. 2.

The indentation hardness of the alumina free Zn−Mn alloy coatings is 420 and 470 MPa for the samples deposited at 40 and 50 mA cm^{-2} respectively. In contrast, the Zn–Mn/Al_2O_3 composite coatings deposited with ultrasonic agitation have significantly higher hardness, in the range between 596 and 680 MPa, depending on the deposition current density. The same trend is observed for the Vickers instrumented hardness. It may be concluded that in case of an ultrasonic agitation, the second-phase particles of alumina in the Zn−Mn coating offer better mechanical properties of composite coatings, which is consistent with other literatures[17,18]. The hardening effect of the Al_2O_3 particles is considered to be related to the two different mechanisms[13]: (1) the role of oxide particles in the alloy matrix as strong obstacles for dislocation movement and (2) grain refinement of the alloy matrix, i.e. the nucleation of small grains on the surface of the incorporated Al_2O_3 particles during the electroreduction process[13,19].

In contrast, the application of the magnetic stirrer in the electrodeposition process of Zn–Mn/Al_2O_3 composite coatings resulted in a decrease of average hardness, although the Al_2O_3 content reached the highest value in the samples, as evidenced by EDS measurements. For these samples, the hardness results were scattered, and several measuring points showed very low hardness values. It may be assumed that the solution agitation by a magnetic stirrer does not ensure a homogeneous dispersion of the alumina

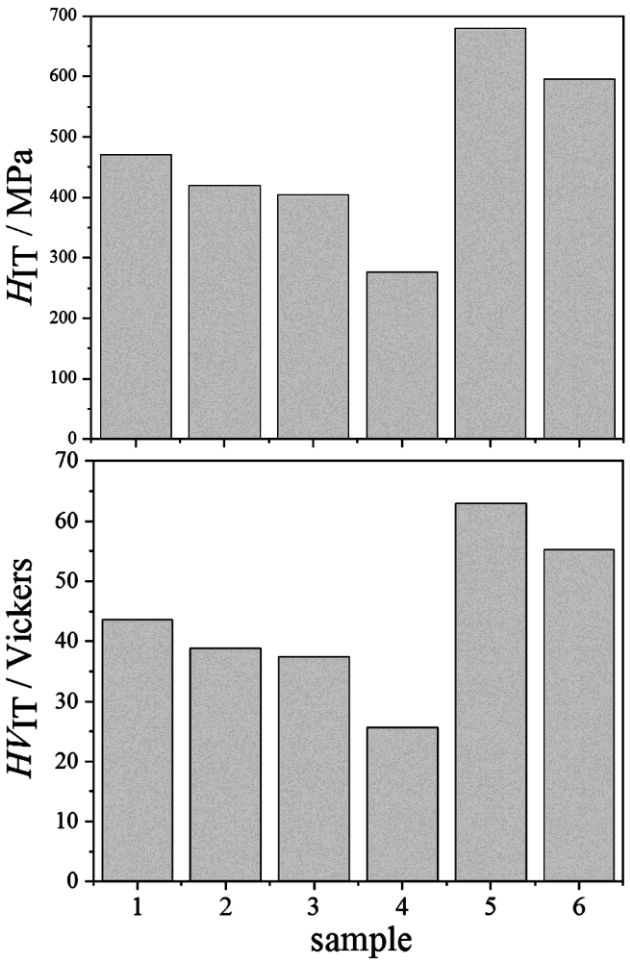

Fig. 2 — Indentation hardness and Vickers instrumented hardness values for Zn−Mn and Zn−Mn/Al_2O_3 coatings produced with different deposition parameters, the samples designation is the same as in Table 1.

particles in the coating (as shown in optical images, Fig. 1), and very low hardness of these samples could be due to formation of microcracks in deposit as a consequence of incorporation of large alumina agglomerates. Earlier it was concluded[17] that the increase in the second phase particle content improves a coating hardness, but only until the coating is compact. And after particles content reaches some limit value, the hardening particles actually worsen the coating microstructure[19,20].

Figure 2 additionally denotes that the increase in the deposition current density, results in improved hardness of the coatings from all three investigated baths (without alumina, with magnetic and ultrasonic agitation). This may be a consequence of the decrease in the crystalline grain size of the coatings, since it is known that the increase in deposition current density results in the grain refinement. The presence of finer grains leads to an enlargement of the grain boundaries, hinders the dislocation motion and thus increases the hardness[13,18,19].

3. 3 Corrosion resistance

The influence of the electrodeposition conditions on the corrosion behavior of the samples was examined by electrochemical impedance spectroscopy in 0.3 wt.% NaCl solution. Figure 3 shows representative Nyquist diagrams that have been obtained at every 24h during the 96h period.

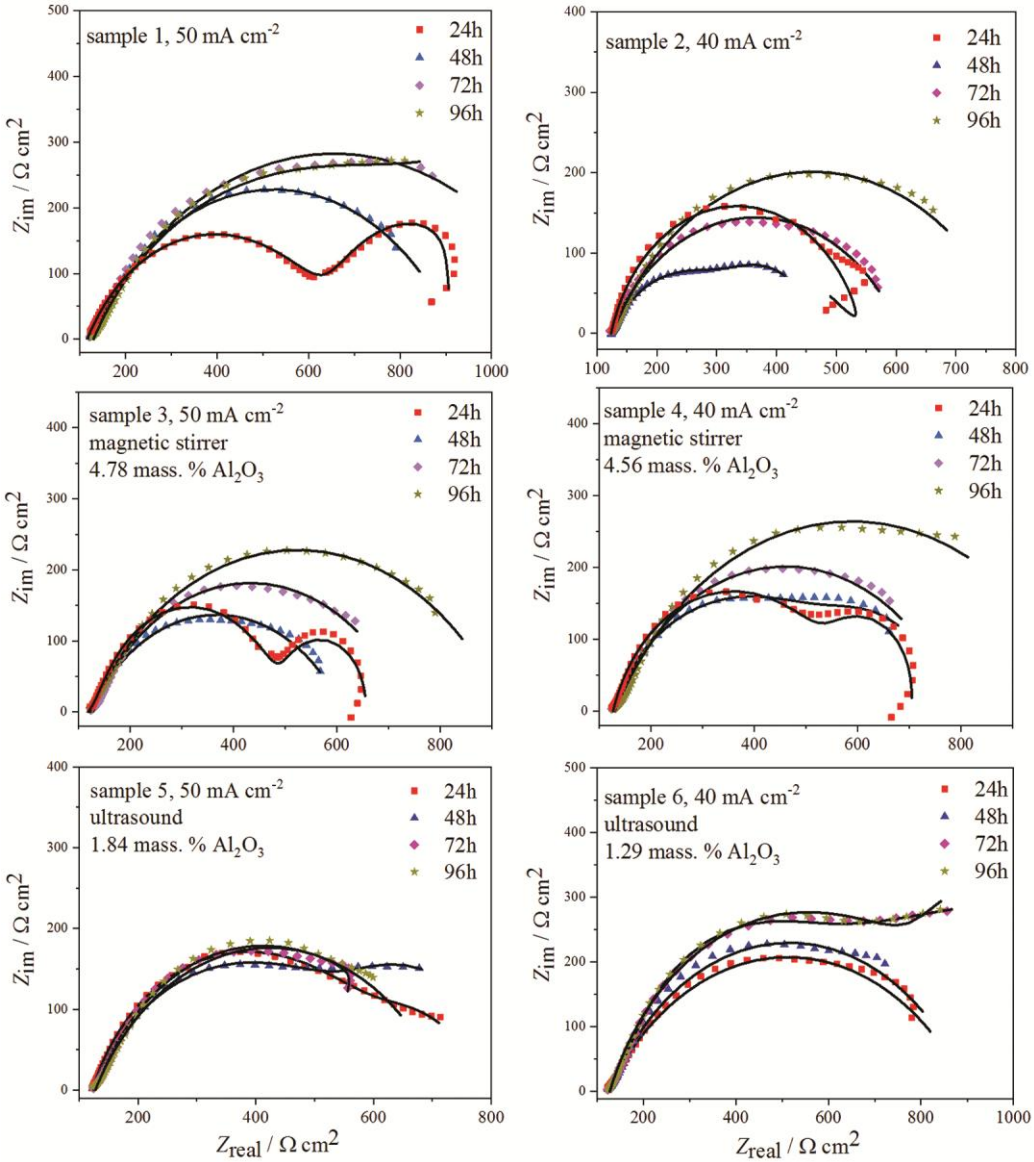

Fig. 3 — Nyquist diagrams of the coatings for various exposure times in 0.3 wt. % NaCl solution.

For majority of the measurements, the Nyquist diagrams contain one depressed semicircle, but for some measurements, the arc recorded at high − middle frequency is followed by the second arc or ill-defined tail. The first arc is related to the charge transfer process, and the low frequency tail indicates a finite thickness layer diffusion process, related to the oxygen reduction[21].

In addition, some spectra recorded during the first 24h, show the so-called inductive behavior at low frequency. Such inductive response is often ascribed to the existence of the inductive element in the equivalent circuit model, which indicates that the rate limiting step in the corrosion process, is the adsorption step[22]. However, new research[23] suggests that the inductive loop observed at low frequencies in Nyquist diagrams is probably not the result of adsorption, but may be a consequence of various other processes. The most common reasons for the appearance of the inductive loop are: a) the charge transfer through the thin, conductive film at the electrode surface, or b) the electrochemical reaction that occurs in two steps, but different time constants are related to these steps. With this approach, the inclusion of the inductive element in the equivalent circuit model is unnecessary, but instead, the fitting procedure may be accomplished by using the model constructed of one or more resistance−capacitance (R−C) couples. In each couple, R and C are in parallel connection, and the couples are connected in series[23].

Based on the previous literature[23], the impedance spectra were fitted with the equivalent circuit model consisting of one or two R−C couples connected in series (Fig. 4). The constant phase element (CPE) was used to describe the non-ideal behavior of the capacitive elements and to obtain higher goodness of fitting[24]. The fitted parameters of the constant phase element were later used to calculate the double layer capacitance values, using Echem Analyst software. Fig. 3 shows high correlation between experimental impedance spectra and the fitting results, presented with solid black lines.

The equivalent circuit with two R−C couples was used only for fitting the spectra with two arcs; with inductive response; or with the ill-defined tail at low frequencies. When the two arcs were observed in the Nyquist diagrams, the attention was given to the resistance value extracted from the arc recorded at high and middle frequencies, that is, according to the previous research of Zn coatings corrosion in NaCl

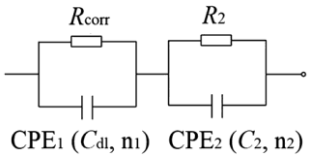

Fig. 4 — Equivalent circuit representing the corrosion process of coating samples in 0.3 wt. % NaCl solution.

medium[21], related to the charge transfer resistance (R_{corr}) of the corrosion process taking place at the metal coating/electrolyte interface.

The parameter values obtained by fitting the recorded impedance spectra, are presented in Table 2 and Fig. 5. Figure 5 shows the R_{corr} values as a function of the immersion time in 0.3 wt.% NaCl solution. For the sake of clearer comparison, the values obtained for the coatings deposited at the same current density are grouped in separate diagrams. It may be noticed that over the investigated period of 96h, the corrosion resistance values increased slightly (from ~400 – 600 to ~600 – 1100 Ω cm^2) for all the coatings. These changes could be mainly ascribed to the evolution of the corrosion product layer that shows a protective ability at Zn−Mn alloy coatings[10]. Although the differences between the R_{corr} values for all samples are rather small, it may be observed that the coating containing Al_2O_3 (sample 6) possesses higher corrosion resistance than alumina-free alloy coatings, while the other samples with alumina particles, such as samples 3 and 4, show the corrosion resistance equal to that of the alumina-free coatings. Zheng *et al.*[3] showed that Al_2O_3 particles increase the corrosion resistance of Zn alloy coatings, and this was attributed to the following reasons: first, Al_2O_3 particles being chemically inert, isolate the alloy matrix from the corrosion medium and decrease its exposed area; second, due to the high electric resistance of alumina particles, they inhibit the corrosion current and decrease the coating corrosion rate, provided they are homogeneously incorporated in the coating[3].

It is important to note that the values of the fractional exponent n of the constant phase element CPE_1 (Table 2), were in the range of 0.60 – 0.80 for all samples, and they slowly decrease over the immersion time. This is an indication that the corrosion process is not purely under activation control, but with the mixed activation-diffusion controlling step. In other words, the metal dissolution occurs through the layer of porous corrosion products at all investigated coatings.[25,26]

Table 2 — Optimum fit parameters for Zn−Mn and Zn−Mn/Al_2O_3 coatings, depending on the immersion time in 0.3 wt. % NaCl

Immersion time (h)	R_{corr}, Ω cm^2	Q_{corr}		R_2, Ω cm^2	Q_2	
		C_{dl}, mF cm^{-2}	n_1		C_2, mF cm^{-2}	n_2
Sample 1						
24	534	1.79	0.67	301	3.34	0.91
48	804	1.25	0.66	-	-	-
72	1070	0.95	0.62	-	-	-
96	820	1.23	0.65	-	-	-
Sample 2						
24	406	2.41	0.84	38	22.72	0.99
48	221	4.38	0.70	116	9.03	0.98
72	487	2.05	0.68			
96	682	1.48	0.73	-	-	-
Sample 3						
24	383	2.53	0.81	161	6.58	0.99
48	491	2.04	0.65	-	-	-
72	611	1.65	0.68	-	-	-
96	778	1.29	0.68	-	-	-
Sample 4						
24	450	1.78	0.8	129	8.18	0.99
48	461	2.16	0.72	178	6.04	0.96
72	671	1.51	0.69	-	-	-
96	919	1.11	0.65	-	-	-
Sample 5						
24	494	2.00	0.74	161	6.71	0.85
48	482	2.02	0.7	201	5.36	0.99
72	557	1.80	0.69	-	-	-
96	593	1.70	0.68	-	-	-
Sample 6						
24	794	1.25	0.72	-	-	-
48	760	1.34	0.66	311	3.44	0.95
72	1346	0.77	0.61	261	4.11	0.99
96	800	1.26	0.75	273	3.91	0.99

As concerning the calculated capacitance values (Table 2) the fitting procedure for majority of the recorded EIS diagrams showed the capacitance values in the range between 1000 and 2000 μF cm^{-2}. Such high capacitance values may be attributed to various factors, like the surface roughness, presence of ceramic particles in the coatings, presence of corrosion products, etc.[27].

In order to additionally characterize the corrosion process of Zn–Mn and Zn–Mn/Al_2O_3 coatings, potentiodynamic polarization curves were recorded for all the samples after their immersion in 0.3 wt. % NaCl solution after a stable open circuit potential was reached (Fig. 6 and Table 3). The cathodic part of the polarization curves again indicated that the corrosion process was under mixed activation-diffusion control, as it was concluded from the impedance spectroscopy. The anodic curves were not related to passivation, and the values of the anodic Tafel slope (~50 mV dec^{-1}) were in correlation with literature data for zinc-based coatings in NaCl solution[21,28,29].

The most important difference between the polarization curves for various samples is the value of the calculated corrosion current density, i.e. the corrosion rate. The composite coating samples electrodeposited with the assistance of ultrasound (samples 5, 6) and the Zn-Mn alloy coating (sample 1) had the lowest corrosion current density, while the composite coatings obtained with magnetic stirring showed higher corrosion rates (samples 3, 4). The corrosion values calculated from the polarization curves differ to some extent from the results of impedance spectroscopy, but it should be held in mind that the former results are related only to the corrosion of freshly immersed samples in NaCl.

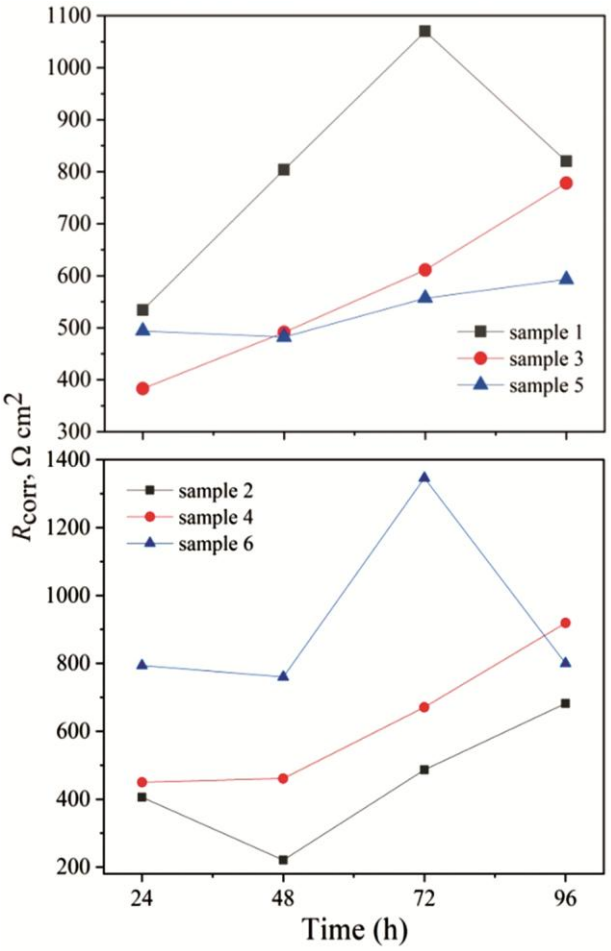

Fig. 5 — Values of corrosion resistance after different exposure times for the samples electrodeposited at 50 mA cm^{-2} (sample 1, 3, 5) and at 40 mA cm^{-2} (sample 2, 4, 6), the samples designation is the same as in Table 1.

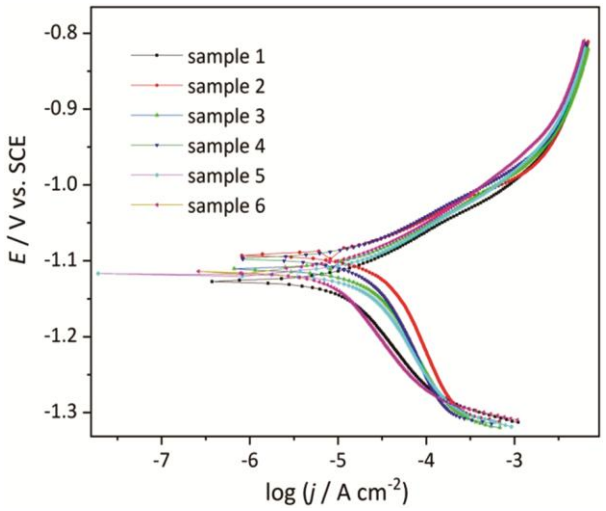

Fig. 6 — Potentiodynamic polarization curves of the Zn−Mn and Zn−Mn/Al_2O_3 coating samples immersed in 0.3 wt. % NaCl solution, the samples designation is the same as in Table 1.

Table 3 — Electrochemical parameters obtained from the potentiodynamic polarization curves

Sample	1	2	3	4	5	6
j_{corr}, μA cm^{-2}	6,29	11,06	10,24	9,71	6,38	4,49
$-E_{corr}$, V	1,128	1,093	1,110	1,096	1,117	1,114

Based on the electrochemical measurements it may be summarized that the corrosion performance of the Zn-Mn/Al_2O_3 coatings deposited under certain parameters, is slightly better or equal to the performance of Zn-Mn coatings.

4 Conclusion

In this work, the electrochemical deposition was applied to achieve a successful production of innovative Zn-Mn alloy coatings combined with alumina particles. The coatings were deposited from a chloride-based electrolyte, without any commercial plating additives. The influence of different deposition current densities and the two agitation techniques on the coating's composition and properties was investigated and based on the results, following conclusions can be highlighted:

- Applied agitation type had significant effect on the weight percentage of the oxide particles incorporated in the alloy deposit: the coatings deposited under mechanical agitation i.e. magnetic stirrer contained 4.5 – 4.8 wt.% Al_2O_3, while those deposited under ultrasonic agitation possessed 1.3 – 1.8 wt.% Al_2O_3.
- The deposition current density did not influence the particles content remarkably.
- The morphology of the composite coatings deposited with mechanical agitation was inhomogeneous, due to particle agglomerates present on the surface (around 50 μm in diameter). However, applied ultrasound during electrodeposition resulted in a significant improvement of the particles dispersion in solution, as well as in the coating. The compactness and grain refinement of the composites was also improved by applied ultrasound, resulting in composite coatings with much better homogeneity and smoothness.
- The electrodeposition with ultrasound agitation was beneficial for the hardness of the examined coatings. The indentation hardness of composite Zn−Mn/Al_2O_3 coatings was increased compared to metal matrix (Zn-Mn alloy).

- The corrosion resistance of the coatings in chloride rich environment was improved when alumina particles were incorporated, but not significantly, and not for all investigated samples.
- The co-deposition of alumina particles, together with ultraso und agitation, showed to be a good way to improve the hardness of the Zn-Mn alloy coatings.

Acknowledgements

This research was financed by the Ministry for Scientific and Technological Development, Higher Education and Information Society, Republic of Srpska (Grant No. 19.032/961-38/19) and by the Ministry of Education, Science and Technological Development of the Republic of Serbia (Contract No. 451-03-9/2021-14/200135).

References

1 Schlesinger M, & Paunovic M, *Modern Electroplating, 5th ed*, (Hoboken, New Jersey, A John Wiley & Sons Inc), 2010
2 Walsh FC, & Ponce de Leon C, *Trans Inst Met Finish,* 92 (2014) 83
3 Zheng M, An M, & Lu J, *Rare Met,* 25 (2006) 174
4 Praveen BM, & Venkatesha TV, *J Alloys Compd,* 482 (2009) 53
5 Peshova M, Bachvarov V, Vitkova S, & Boshkov N, *Trans Inst Met Finish,* 98(2) (2020) 73
6 Arora S, Sharma B, & Srivastava C, *Surf Coat Technol,* 398 (2020) 126083
7 Abdel Hamid Z, *Anti-Corros Methods Mater, 48* (2011) 235
8 Boshkova N, Lutov L, & Boshkov N, *J Int Sci Publ:Mater Methods Technol,* 12 (2018) 266
9 Bučko M, Rogan J, Jokić B, Mitrić M, Lačnjevac U, & Bajat JB, *J Solid State Electrochem*, 17 (2013) 1409
10 Bučko M, Rogan J, Stevanović SI, Perić-Grujić A, & Bajat JB, *Corros Sci*, 53 (2011) 2861
11 Suzuki Y, Wajima M, & Asai O, *J Electrochem Soc*, 133 (1986) 259
12 Mulukutla M, Singh A, & Harimkar SP, *Trans Inst Met Finish,* 90 (2012) 316
13 García-Lecina E, García-Urrutia I, Díez JA, Morgiel J, & Indyka P, *Surf Coat Technol*, 206 (2012) 2998
14 Wielage B, Lampke T, Zacher M, & Dietrich D, *Key Eng Mater*, 384 (2008) 283
15 Riđošić M, Salicio-Paz A, García-Lecina E, Zabinski P, Živković LS, & Bajat JB, *JMR&T, in press* https://doi.org/10.1016/j.jmrt.2021.05.064.
16 Tudela I, Yhang Y, Pal M, Kerr I, & Cobley A J, *Surf Coat Technol*, 259 (2014) 363
17 Chen W, & Gao W, *Electrochim Acta*, 55 (2010) 6865
18 Kartal M, Buyukbayram I, Alp A, & Akbulut H, *Mater Today: Proc*, 4 (2017) 6982
19 Kamnerdkhag P, Free M L, Shah A A, & Rodchanarowan A, *Int J Hydrog Energy*, 42 (2017) 2078
20 Akhtar K, Khan ZU, Gul M, Zubair N, & Ali Shah S S, *J of Materi Eng and Perform*, 27 (2018) 2827
21 Barranco V, Feliu S Jr, & Feliu S, *Corros Sci* 46 (2004) 2203
22 King A D, Birbilis N, & Scully J R, *Electrochim Acta*, 121 (2014) 394
23 Klotz D, *Electrochem Commun*, 98 (2019) 58
24 García-Antón J, Fernández-Domene RM, Sánchez-Tovar R, Escrivà-Cerdán C, Leiva-García R, García, & Urtiaga A, *Chem Eng Sci*, 111 (2014) 402
25 Amand S, Musiani M, Orazem ME, Pébère N, Tribollet B, & Vivier V, *Electrochim Acta*, 87 (2013) 693
26 Córdoba-Torres P, Mesquita TJ, & Nogueira RP, *J Phys Chem C*, 119 (2015) 4136
27 Kiselev VG, Sergeev VV, & Rouzich EN, *Corros Rev*, 35 (2017) 47
28 Arunima SR, *Asian J Chem*, 36 (2020) 1370
29 Kania H, Saternus M, Kudláček J, & Svoboda J, *Coatings*, 10 (2020) 758